Diffraction pattern of a defect: Two-dimensional angular correlation of positron-annihilation radiation studies of defects in semiconductors

T. McMullen and Marilyn F. Bishop
Department of Physics, Virginia Commonwealth University, Richmond, Virginia 23284-2000
(Received 21 November 1995; revised manuscript received 22 October 1996)

Electron-positron momentum spectra of defects in semiconductors contain more information about the nature of the defects than has been recognized previously. Diffraction patterns that arise both from the nature of the electronic states and from the geometric structure can be seen in the simulated two-dimensional angular correlation of annihilation radiation spectra for positrons annihilating at a model vacancy in a tetrahedrally coordinated semiconductor. These should be experimentally observable in high-resolution spectra. [S0163-1829(97)02507-1]

We present model calculations that show that detailed information about the electronic and geometric structure of defects can be obtained from two-dimensional angular correlation of annihilation radiation (2D ACAR) spectra originating from positrons trapped at defects. This is because the e^--e^+ momentum spectrum from a defect-trapped positron is, basically, the diffraction pattern of the defect. Information about the detailed structure of defects in semiconductors is difficult to obtain and requires a variety of techniques. This information is, nevertheless, extremely useful in controlling the properties of materials for use in semiconductor devices. This work shows that 2D ACAR is a valuable addition to the available techniques.

Positron annihilation (PA) has been used extensively to study both the electronic structure of crystalline materials and the properties of defects in metals and semiconductors. Variable energy positron beams (VEPB's) allow PA techniques to be used as depth-profiling methods with sub-μm resolution over depths down to several μm below the surface. At a few facilities, these beams are becoming intense enough for depth-sensitive 2D ACAR measurements to be made, so that epilayer materials, interfaces, and multilayer structures can be studied.[1]

Until recently, high-resolution e^--e^+ momentum spectroscopy using 1D and 2D ACAR techniques have been used only for Fermi-surface investigations in defect-free materials. Although defects have been studied extensively by PA, this has been done using only the lower-resolution momentum technique of Doppler broadening, and by e^+ lifetime measurements.[2,3] An interesting question is to what extent detailed structure of defects can be extracted from 2D ACAR data, or if the uncertainty principle momentum broadening that would result from the localization of the positron and the falloff of electron wave functions on the scale of a point defect obscure structural information. We will show in this paper that more detailed information can be extracted from 2D ACAR than has previously been appreciated.

By the electronic structure we mean the charge state and the nature of the occupied orbitals at the defect. The arrangement of the neigboring atoms, including lattice relaxation and symmetry-lowering distortions, is called the geometric structure. The electronic and geometric structures can be closely related, as in the ''large lattice relaxation'' class of defects such as $EL2$ and DX, where changes in the charge state drive the large geometric rearrangements. A simple model based on vacancies in tetrahedrally coordinated semiconductors is used to show how the diffraction pattern produced by the electronic and geometric structure of a defect appears in an e^--e^+ momentum spectrum. This pattern arises from the phase correlations and occupancy of the valence states around the defect.

A 2D ACAR spectrum is a two-dimensional projection of the three-dimensional e^--e^+ momentum density $n(\mathbf{p})$. We consider a model in which the electron and positron states are each represented by a single spherically symmetric Gaussian. Even though the valence orbitals in semiconductors are sp^3 hybrids, this model illustrates the basic structure that would appear in simulations using more complete basis sets. In formulating the model, we suppose that the positron is trapped in a vacancy at the origin, with the e^+ state $|\varphi_+\rangle$ an s Gaussian with decay parameter α_0. In addition, we represent an atomic orbital centered on each of the ith neighboring atoms located at $\mathbf{R}_i$ by a Gaussian with decay parameter α_i. If the electron states are a linear combination of these Gaussian atomic orbitals,

$$|\psi_j\rangle = \sum_i a_i^{(j)} |\varphi_i\rangle, \tag{1}$$

the momentum density is the superposition of contributions from each of these,

$$n(\hbar\mathbf{k}) = \sum_j n^{(j)}(\hbar\mathbf{k}), \tag{2}$$

where

$$n^{(j)}(\hbar\mathbf{k}) = \left| \int d^3r e^{i\mathbf{k}\cdot\mathbf{r}} \varphi_+(\mathbf{r}) \psi_j(\mathbf{r}) \right|^2 \tag{3}$$

is the contribution of the jth electron state $|\psi_j\rangle$. The individual integrals needed are the momentum amplitudes,

$$f(\mathbf{k}|\alpha_i, \mathbf{R}_i) \equiv \int d^3r e^{i\mathbf{k}\cdot\mathbf{r}} \varphi_+(\mathbf{r}) \varphi_i(\mathbf{r}), \tag{4}$$

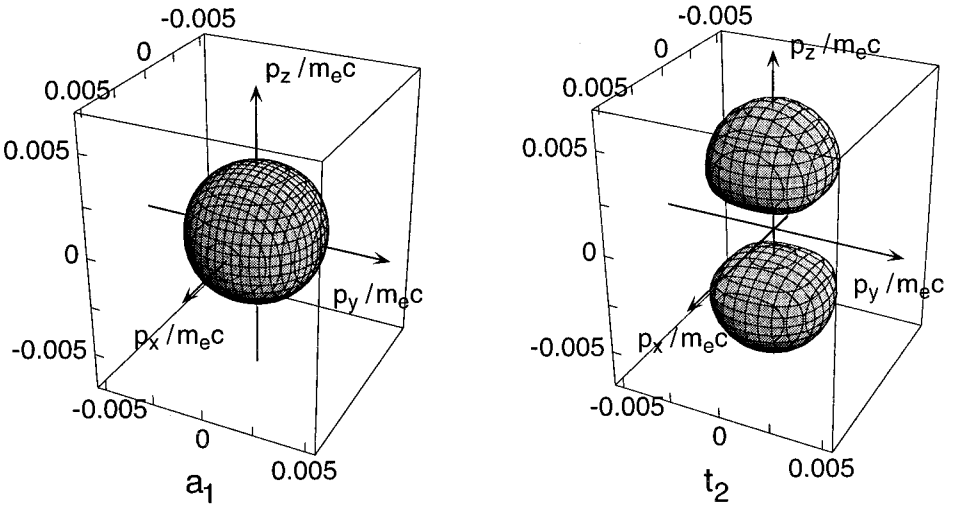

FIG. 1. Contours of constant momentum density $n^{(j)}(\mathbf{p})$ for the a_1 and t_2 states. The momentum $\mathbf{p}$ is given in multiples of $m_e c$ for a lattice parameter of 5.65 Å.

and the contributions to the momentum density may be written in terms of these as

$$n^{(j)}(\hbar\mathbf{k}) = \left| \sum_i a_i^{(j)} f(\mathbf{k}|\alpha_i, \mathbf{R}_i) \right|^2 . \tag{5}$$

The simplicity of this model is now evident, since the integral (4) can be evaluated analytically for Gaussians with the result

$$f(\mathbf{k}|\alpha,\mathbf{R}) = \left(\frac{2\alpha_0\alpha}{\alpha_0^2+\alpha^2} \right)^{3/2} \exp\left(-\frac{\alpha_0^2\alpha^2}{\alpha_0^2+\alpha^2} R^2 \right) \times \exp\left(-\frac{k^2}{4(\alpha_0^2+\alpha^2)} \right) \exp\left(\frac{\alpha^2}{\alpha_0^2+\alpha^2} [i\mathbf{k}\cdot\mathbf{R}] \right). \tag{6}$$

The spatial extent of the orbitals is reflected in the falloff of the momentum space Gaussian in this expression. The symmetry of the defect electronic state gives rise to an interference that can be seen in the cross terms in Eq. (5).

To illustrate how this information is contained in the e^--e^+ momentum density, we chose the Gaussians to mimic roughly a positron trapped at the vacancy $V_{\mathrm{As}}{}^-$ in GaAs. In order to choose appropriate Gaussians, we computed the positron density for a positron trapped at an ideal (i.e., undistorted) negative As vacancy using a superimposed ion potential and a local e^+-e^- correlation potential.[2,4–8] The e^+ density falls off more sharply in the direction of a neighbor than it does in the opposite direction, with the best Gaussian fits in these two extreme directions given by $\alpha_0 a_0 \simeq 0.32$ and $\alpha_0 a_0 \simeq 0.19$, where $a_0 = 0.529$ Å is the Bohr radius. The model used here requires spherically symmetric Gaussians, so we chose the Gaussian decay parameter $\alpha_0 a_0 = 0.22$ as a compromise. For the electrons, we computed the $4s$ and $4p$ wave functions for a Ga^0 atom using the local spin density approximation. The radial wave functions were represented well in the outer overlap region beyond $\sim 1.5 a_0$ by single Gaussians with decay parameters $\alpha a_0 = 0.38$ for the $4s$ and $\alpha a_0 = 0.26$ for the $4p$. We used the average, $\alpha_i a_0 = 0.32$, for the four neighboring atoms in our model.

An ideal vacancy in a semiconductor with a diamond or zinc-blende structure has four neighbors. Its ionization levels correspond to filling the lower-energy a_1 states and the higher-energy t_2 states.[9] The a_1 state can hold two electrons, and the t_2 states can hold six. In GaAs, for example, the neutral As vacancy lacks the five As electrons that provide a complete octet in the perfect crystal. Three electrons remain in the a_1 and t_2 linear combinations formed from the dangling bonds. Thus, the a_1 states are filled with two electrons, and the remaining electron is in a t_2 state. The singly negative vacancy $V_{\mathrm{As}}{}^-$ has one more electron in the t_2 state.

The symmetry of these states is reflected in the momentum density and hence the 2D ACAR spectrum. Figure 1 compares the surfaces of constant momentum density $n^{(j)}(\mathrm{p})$ for the a_1 state

$$\frac{1}{2\sqrt{1+3S}} (|\varphi_1\rangle + |\varphi_2\rangle + |\varphi_3\rangle + |\varphi_4\rangle) \tag{7}$$

and the t_2 state

$$\frac{1}{2\sqrt{1-S}} (|\varphi_1\rangle - |\varphi_2\rangle - |\varphi_3\rangle + |\varphi_4\rangle), \tag{8}$$

where S is the overlap integral, calculated using our model with the parameters given above. The atoms $1, \ldots, 4$ have coordinates $(1,1,1)$, $(1,-1,-1)$, $(-1,1,-1)$, $(-1,-1,1)$ times $a/4$, where $\hat{x}$, $\hat{y}$, and $\hat{z}$ are along the crystal axes and $a = 5.65$ Å for GaAs. Both constant momentum density contours are in the relatively low momentum region, with that for the a_1 state at 1/4 of the maximum central peak, and that for the t_2 state around 1/3 of its maximum.

The momentum space symmetries shown in Fig. 1 are dramatically different because of the symmetries (7) and (8) of the spatial orbitals. The total momentum density is the superposition (2) of contributions from the occupied electronic states. Changing orbital occupancies, i.e., charge states

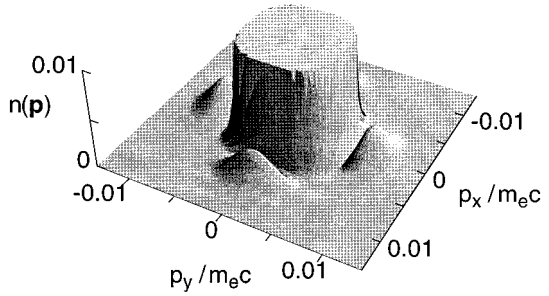

FIG. 2. The momentum density $n^{(a_1)}(\mathbf{p})$ in the $p_z=0$ plane for the a_1 state showing an enlarged view of the structure at $0\rightarrow 1\%$ of the peak height. This structure gives the separation of neighboring atoms. The momentum $\mathbf{p}$ is given in multiples of $m_e c$ for a lattice parameter of 5.65 Å.

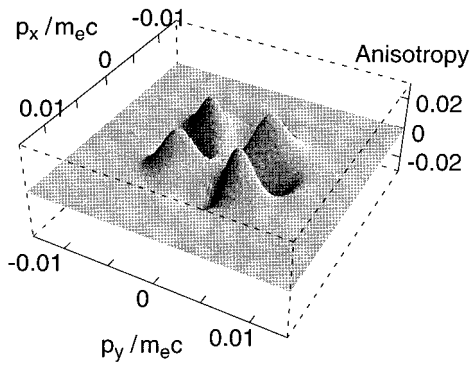

FIG. 3. Anisotropy in the 2D ACAR spectrum for the a_1 state. The anisotropy is given as a fraction of the height of the central peak of the 2D ACAR spectrum. The momentum $\mathbf{p}$ is given in multiples of $m_e c$ for a lattice parameter of 5.65 Å.

of the defect, will alter their weightings in the total momentum density. As levels become filled, there may be cancellations analogous to those from a filled band in a solid. When there are various orientations of degenerate levels, it may be necessary to strain the sample to see clear signatures of the electronic state symmetries.

Geometric information lies in the higher momentum region. This comes from the

$$\left| \sum_i a_i^{(j)} \exp\left(\frac{\alpha^2}{\alpha_0^2+\alpha^2} [i\mathbf{k}\cdot\mathbf{R}_i] \right) \right|^2 \tag{9}$$

interference term in Eqs. (5) and (6). To illustrate, Fig. 2 shows a $p_z=0$ cut through our model e^--e^+ momentum density for the a_1 state. The entire peak appears more or less circularly symmetric, and at 1/4 of the maximum height is just the $k_z=0$ circle on the sphere of Fig. 1 (a_1 state). Figure 2 shows an expanded scale in which the low intensity structure ($\leqslant 1\%$ of maximum) out in the higher momentum tails is evident. The square pattern of troughs results from the minima caused by the interference term (9), which gives

$$n^{(a_1)}(\hbar k_x \hat{x} + \hbar k_y \hat{y}) \sim \cos^2\left(\frac{\alpha^2}{\alpha_0^2+\alpha^2} \frac{k_x a}{4} \right), \tag{10}$$

and has nodes at

$$\frac{\alpha^2}{\alpha_0^2+\alpha^2} \frac{k_x a}{4} = \left(n+\frac{1}{2} \right) \pi, \tag{11}$$

and similarly for k_y. The first of these values is, for our parameters, at $k_x, k_y \simeq 9.25/a \simeq 6.3\times 10^{-3} m_e c/\hbar$, and is the origin of the structure shown in Fig. 2.

A 2D ACAR measurement gives the two components of momentum that lie in a plane normal to the line joining the two detectors. Consequently, a 2D ACAR spectrum is the result of line integrals in momentum space in the direction joining the detectors. The structure resulting from the interference term (10) is most pronounced when the integration line passes along maxima or minima. The experimental consequences are illustrated in Fig. 3, which shows the anisotropy in the simulated 2D ACAR spectrum. The dip at $\sim 6.3\times 10^{-3} m_e c$ comes from the troughs in Fig. 2. Anisotropy resembling that of our model (Fig. 3) can be seen in the data already reported by Ambigapathy *et al.*,[10,11] Manuel *et al.*,[12] and Peng *et al.*[13] for the experimental 2D ACAR spectra for positrons trapped at vacancies in GaAs. For example, the basic structure of peaks in Fig. 11 of Ref. 10 is the same as we obtain for that orientation, which is a projection of the momentum density into a plane perpendicular to the [110] direction. The projection shown in Fig. 3 is into a plane perpendicular to [001] instead, because that most clearly shows the structure arising from the minima.

We next ask what is required for an experiment to observe this geometric structural information in the 2D ACAR spectrum. Suppose that one wished to have sufficiently good statistical resolution to detect the change in this structure that would result from a 1% relaxation of the nearest neighbors about the vacancy. Using the simulated spectrum presented in this paper, this change in the nearest-neighbor separation produces, relative to the intensity at $\mathbf{p}=0$, a $\sim 0.5\%$ change in the 2D ACAR spectrum around $6\times 10^{-3} m_e c$. The core contribution, which is $\sim 10\%$ of the total annihilation rate, but with a momentum width that is 10 times that of the valence electrons, is negligible in comparison at this momentum. In our simulation, the magnitude of the 2D ACAR spectrum at $\sim 6\times 10^{-3} m_e c$ is $\sim 1\%$ of the intensity at $\mathbf{p}=0$. Because of this, we suppose that a statistical resolution of $\pm 5\%$ in the channels in this momentum region is sufficient. The probability that n positrons annihilate in a momentum channel $(\Delta p)^2$ follows the Poisson distribution, so that the counting error in each square momentum bin is $\pm 1/\sqrt{n}$. This means that in this momentum bin we need a statistical resolution of 1 in 20, or a total number of counts of 400. Let us assume the same histogram bin size as in Refs. 10 and 11 of 401×401 bins of size $0.15\times 0.15 (10^{-3} m_e c)^2$ over an angular range of $60\times 60 (10^{-3} m_e c)^2$. This means that the total number of counts in the entire spectrum needs to be about 2×10^8, the same order of magnitude as in Refs. 10 and 11. Measurements of small changes in structure, such as a 1% relaxation of the atoms neighboring a vacancy, seem entirely feasible.

The structures in 2D ACAR spectra that contain this geometric information do have quite low intensities, and would be clearer if the full three-dimensional momentum density were reconstructed from measurements in differently ori-

ented planes. Although this would be experimentally challenging, the wealth of information obtained would be well worth the effort.

The pattern shown in Fig. 2 will be recognized as a part of the Fourier transform of a tetrahedron. Equations (5) and (6) show that, in general, the e^--e^+ momentum density is the Fourier transform of the neighbors, with form factors arising from the orbital coefficients $a_i^{(j)}$ and the nature of these orbitals. Since the diffraction pattern of an object is its Fourier transform, the e^--e^+ momentum density for a vacancy-trapped e^+ is the diffraction pattern of the defect. The interpretation of this diffraction pattern is not totally straightforward, because the transform involves not just $\exp(i\mathbf{k}\cdot\mathbf{R}_i)$, but $\exp(iA\mathbf{k}\cdot\mathbf{R}_i)$, where A is a scale factor as in Eq. (9) containing wave-function coefficients. This means that computer simulation, with realistic electronic structure information, will be needed to interpret the data properly.

A better representation of the wave functions requires multiple Gaussians. These will smear out the structure to some extent, because they produce different scale factors A. We expect the structure to survive, because the e^+ samples the outer regions of the atoms, and the wave functions in the *outer* regions are represented quite well by the single Gaussians used here. It is possible to find a generating function for the Fourier transforms of higher angular momentum Gaussians, so the simple *s* Gaussian model described here can be extended to realistic electron e^- and e^+ states by using Gaussian basis sets,[14,15] with no need for numerical multidimensional Fourier transformation. This should give an efficient computer simulation procedure for the interpretation of 2D ACAR spectra. Although the calculations presented here do not include corrections for the many-body enhancement of the annihilation rate, these have been shown to have a relatively weak momentum dependence,[16,17] at least for the electron gas.

Because electron-positron momentum spectra from defect-trapped positrons give diffraction patterns of defects, 2D ACAR is a promising tool for the study of the electronic and geometric structures of defects. Our simple *s* Gaussian model illustrates how the nature of the electronic states and the geometry of the atoms neighboring the defect is reflected in the 2D ACAR spectra. The most important features are that the overall shape gives the symmetry of the electronic state, and patterns in the higher momentum tails are related to the geometry of the neighbors.

We are grateful to D. R. Harshman and K. G. Lynn for urging us to think about defect ACAR, and for helpful discussions. R. M. Nieminen pointed out the similarity of our computed anisotropies to the measurements reported in Ref. 11, and A. A. Manuel kindly provided a copy of Ref. 11. This work was supported in part by Brookhaven National Laboratory under BNL Contract No. 736928.

[1] P. J. Schultz and K. G. Lynn, Rev. Mod. Phys. **60**, 701 (1988).
[2] M. J. Puska and R. M. Nieminen, Rev. Mod. Phys. **66**, 841 (1994).
[3] ACAR was used in a study of vacancies in metals by M. J. Fluss, S. Berko, B. Chakraborty, P. Lippel, and R. W. Siegel, J. Phys. F **14**, 2855 (1984).
[4] M. J. Puska and R. M. Nieminen, J. Phys. F **13**, 333 (1983).
[5] M. J. Puska and R. M. Nieminen, Phys. Rev. B **29**, 5382 (1984).
[6] E. Boronski and R. M. Nieminen, Phys. Rev. B **34**, 3820 (1986).
[7] M. J. Puska, S. Mäkinen, M. Manninen, and R. M. Nieminen, Phys. Rev. B **39**, 7666 (1989).
[8] T. McMullen *et al.*, Phys. Rev. B **43**, 10 422 (1991).
[9] U. Scherz and M. Scheffler, in *Imperfections in III/V Materials*, edited by E. R. Weber (Academic Press, San Diego, 1993).
[10] R. Ambigapathy *et al.*, Phys. Rev. B **50**, 2188 (1994).
[11] R. Ambigapathy, Travail de Diplôme, Universite de Geneve, 1994.
[12] A. A. Manuel *et al.*, J. Phys. (France) IV **5**, C1 (1995).
[13] J. P. Peng *et al.*, Phys. Rev. B **50**, 11 247 (1994).
[14] S. F. Boys, Proc. R. Soc. London **A200**, 542 (1950).
[15] Extensive references to Gaussian methods are given and a contemporary implementation is described in the documentation for the programs GAUSSIAN 94, especially in M. J. Frisch, A. Frisch, and J. B. Foresman, *Gaussian 94 User's Reference* (Gaussian, Inc., Pittsburgh, 1995).
[16] J. Arponen and E. Pajanne, Ann. Phys. (N.Y.) **121**, 343 (1979).
[17] J. P. Carbotte, *Positron Solid State Physics* (Soc. Italiana di Fisica, Bologna, Italy, 1983), Vol. LXXXIII Corso.